Aspects on Remote Sensing assisted Wind Farm Minute-Scale Forecasting

Johan Arnqvist[1,2] Jess U. Jørgensen [3], Corinna Möhrlen [3]*

[1] *Uppsala University, Department of Earth Sciences, Unit of Air Water and Landscape sciences, Uppsala, Sweden*
[2] *RISE Research Institutes of Sweden, Department of Electrification and Reliability, Unit of Renewable Energy Systems, Karlstad, Sweden*
[3] *WEPROG ApS, Drejervaenget 8, 5610 Assens, Denmark*
* *johan.arnqvist@geo.uu.se*

Keywords: SODAR, REMOTE SENSING, WINDPOWER FORECASTING, . . .)

Abstract

The larger share of non-scheduled renewable energy in the electricity mix is not only subject to forecast uncertainty, but also increases volatility in the electricity markets. The motivation behind the present work is the desire to operate wind farms proactively, and facilitate participation on intra-hour balancing markets which requires precise forecasts with minimal uncertainty. The aim is to contribute to further understanding of the benefit and limitations of using independent site measurements of wind speed to assist forecasts of the available power. Specifically, the study investigates how the time of availability and distance to target location of the observation impacts the skill of the forecast. To achieve this the study has used a 180 m tall mast and 7 AQ510 SODARs placed at varying distances from the met-tower in combination with a 5-member high resolution numerical weather prediction ensemble.

1 Introduction

As the penetration level of renewables grow, managing, balancing and keeping enough reserves on the grid offers challenges. A recent report by the International Energy Agency concluded that already in phase four (out of six), where penetration levels are above 35% and up to 75% of variable renewable energy (VRE) in annual generation, challenges in stability and flexibility across all timeframes become more acute [1]. Part of the solution, currently being implemented in many of those electricity markets with high portions of VRE, is the participation of traditionally non-dispatchable renewable energy in balancing services. Active participation of wind power requires accurate minute to hour-scale forecasting [2]. Similar forecasts are crucial to understand the constantly varying need for activation of balancing services to meet departures from production plans. As input to such forecasts, power measurements are usually insufficient [3], whether this is in relation to clouds at solar plants or wind speeds at wind farms. At wind farms, it is often related to the absence of information about wind conditions above cut-out (full load) or below cut-in (no production). In both cases, power data fails to indicate forecast trends or biases, which may stem from e.g. high winds or icing. Additionally, in curtailed operation, power measurements do not inform on the potential power and the nacelle-anemometer transfer function is out of its normal condition. Because of this, wind farms should ideally be complemented with independent wind measurements. With modern turbines now exceeding 150m (250-300m in low-wind areas)[4, 5], traditional met masts are increasingly infeasible due to costs and required planning permission. Remote sensing tools like SODARs, LIDARs or RADARs are attractive alternatives offering real-time wind profiles and turbulence data[6–9]. However, deploying these instruments in new environments poses challenges:

- Lead time: How much added value does the remote sensor contribute with depending on lead time
- Spatial validity: How useful is the remote sensor depending on the distance to the target location
- Reliability: How is predictability impacted when the data stream is lost?
- Handling of missing data : When data gaps appear in the observations, what alternatives are there?

To address impacts of weather-related and real-time gaps on forecasting challenges as well as data quality issues, we use a 5-member WEPROG MSEPS ensemble NWP, matching forecasts to recent observations in time and space.

1.1 The forecasting challenge

To facilitate active participation on the minute to hour scale balancing market by wind energy, the wind power potential must be estimated with a lead time in the order of 15 to 60 minutes. Even if wind energy does not participate in balancing services, the difference between production plans submitted day-ahead and most likely real time production is desired to be known 15-60 minutes in advance so that appropriate balancing power can be activated. Regarding the time resolution of the forecasts themselves, this also depend on the market, but is on the minute scale. In this study, 10 minute segments are applied. The complicated process of gathering, harmonizing and assimilating observational data means that traditional NWP will inevitably

be somewhat outdated by the time a forecast is issued. Moreover, the resolution of NWP for wind energy purposes, >1 km, means that fluctuations on the scale of the forecasting problem is reduced, in addition to having little to none predictability. To overcome these challenges, a forecasting methodology that combines NWP input with local observations using a statistical/empirical method is commonly adopted [10]. The aim of this publication is to explore such a setup using local SODAR observations in combination with a typical NWP product from a theoretical perspective.

2 Methodology

The following describes the site of the experiment, the observational data, the model-setup, how the prediction error can be decomposed to highlight different error sources and a simplified prediction methodology by blending NWP forecasts with observations.

2.1 Site

The Hornamossen measurement campaign was undertaken in 2015-2017 as part of a Swedish project aimed at better understanding aspects of wind energy in forested landscapes [11]. In addition to observations in a 180 m tall meteorological mast, a shorter campaign under the New Eurpean Wind Atlas project included 10 remote sensors spread out on an east-west segment of approximately 10 km length [12]. A map of the site topography is displayed in Figure 1 together with the location of the measurement tower and the remote sensors used for this study.

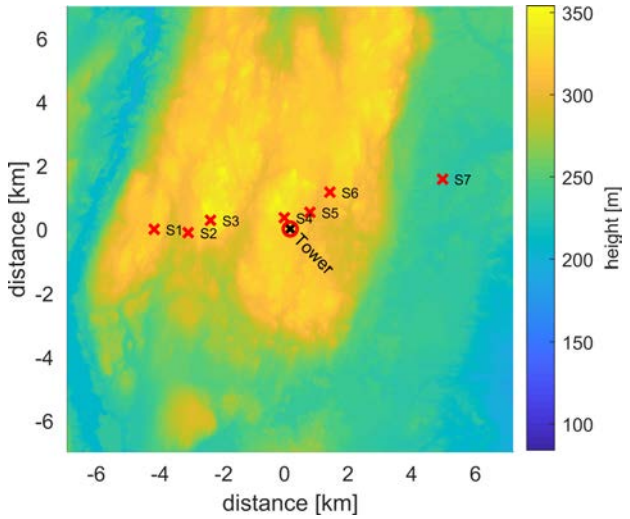

Fig. 1 Elevation map from the Hornamossen measurement site. The locations for the 7 SODARs are marked with red crosses

2.2 Measurements

The measurement tower was operated between may 2015 and may 2017 and had 10 levels of cup anemometers (Thies 1:st class) between 40 and 180 m and 8 levels of sonic anemometers (Metek USA-1) between 21 and 173 m. The SODAR measurements was collected using 7 AQ510 SODARs from AQ System. The SODARs were measuring the wind profile between 40 and 200 m and before the deployment at each location they were briefly tested close to the tower to verify that they were functioning correctly. The SODAR campaign lasted between April and mid August 2016, apart from one SODAR which was deployed in late June and one which was running intermittently most of 2016. The data availability is reported in Table 1 for the concurrent heights with the NWP simulations. For studying the correlations, concurrent data for each unit at 100 m height was used (apart from the vertical cross correlation where only full profiles were considered). To study the spectral statistics data-gaps were filled with linear interpolation (SODAR S5, height 100 m). Spectral statistics where then determined through temporally averaging a Morlet wavelet decomposition of time scales ranging from 30 days to 30 minutes using decomposition scripts from [13].

Table 1 Availability of the 7 SODAR units [%]. SODAR S3 and S4 were run intermittently during the period which explains their lower availability

Height	S1	S2	S3	S4	S5	S6	S7
40	95.8	97	69.4	77.8	95.4	93.7	96.7
100	93.5	95.5	69.9	74.5	91	91.7	95.3
170	80.7	82.3	61.5	62	69.8	73.2	81.7

2.3 Model description

We have performed a mini ensemble simulation using model techniques optimized for high spatial- and time resolution, configured with emphasis on simulating variability. The main objective of this study was to carry out a detailed simulation of the wind speed and direction in altitudes from 40 to 170m in 10 minute time resolution. The experiment was designed to clarify, whether the observed variability can be explained by processes taking place within a 180km model domain. In other words, does the 10 minute variability grow and decay in high resolution models to the observed level ?.

The simulation was chosen as a downscaling from a large-scale analysis. In previous experiments of similar kind (e.g. at the DTU Test center Østerild [14]), it was found that the skill of the simulation was highest with grid spacing of approximately 2.5km. Further resolution increases did not improve the Østerild simulation. In this case, the remote sensing equipment was located at significant distances relative to the mast. The model output was therefore computed in 10 minute intervals for each of the 8 locations with vertical interpolation to fixed height above ground.

The model setup consists of a nested model system with one outer boundary member in 22km grid resolution with 32 levels in the vertical. This member uses 6-hourly analysis from NCEP's global forecast model (GFS)[15] as lateral boundary conditions and as large-scale increments. This model provides hourly lateral boundary values to 5 High-Resolution (HR)

members running with 60 levels in a 1.5km grid. This means, the difference between the HR members is only caused by the differences in the formulations of the HR members. The external forcing is the same for each HR member.

The five numerical weather prediction (NWP) models used in the experiment were selected from the 75 member Multi-scheme Ensemble Prodiction System (MSEPS) [16], where each member uses different sets of condensation and vertical diffusion schemes. All five ensemble members used Eulerian Advection with a time step of 8 seconds, using the hydrostatic approximation. The physical parameterization routines were computed every 80 seconds. This means that there were 75 dynamic time steps every 10 minutes and 7 or 8 physical time steps. The post-processing output was generated upon completion of each physical time step.

We applied a schedule with one daily run with a 24 hour forecast horizon for the entire nested model system. The five chosen ensemble members differ from each other already from the first model time step, because the first guess from the previous day is blended with large-scale analysis and boundary values from NCEP's global GFS model. The model area contains more than 4000 grid points per large-scale NCEP grid point. This means that the first guess from the MSEPS ensemble member models contain each important details, which is not present in the NCEP analysis data.

Each of the five high-resolution ensemble members uses the same roughness and orography. The roughness input data was in fact used to generate higher orography rather than following the original terrain orography. This decision was taken, because the flow in subgrid scale valleys is driven by orography details, which are not resolved in the 1.5 km grid. A NWP model assumes that the grid scale input data can be regarded as the average value for each cell in the model grid. This means that the shape and position of near grid-scale obstacles generate fictive flow. Such fictive flow will have incorrect impact on the flow at higher altitudes in neutral and unstable conditions. Effectively, we replace small scale roughness located in valleys partially with solid earth. Therefore, the net flux of momentum, heat and moisture is handled in the surface parameterization of the physical parameterization at a virtually smooth surface. Hence, the friction is applied at a higher altitude, which is fundamentally different from reality. In the model's coordinate system, the numerical stability of the vertical diffusion process however increases, because there, the number of steep slopes is reduced. This methodology is hence optimized for numerical stability and to simulate flow on top of so-called grid-scale hills and mountains, but implies compromises near the surface inside valleys. Compared to using a mean orography, the lee waves will be developed stronger, because of a stronger blocking of the obstacle, which resembles the natural world.

2.4 Temporal scales

To assist the interpretation of potential forecast errors we decompose the wind speed, as measured or simulated, into

$$u = \overline{u} + u', \tag{1}$$

where u is the instantaneous wind speed, $\overline{u}$ is the temporally averaged wind speed in segments T long relevant for the forecasting (in this study we use $T = 10$ minutes) and u' is the fluctuations on timescales smaller than T. Furthermore, we apply a similar decomposition for the long term mean wind at the site

$$\tilde{u} = \overline{u} - \langle \overline{u} \rangle \tag{2}$$

where $\tilde{u}$ is the fluctuation away from the long term temporal average, represented by $\langle\ \rangle$, taken over time $\mathcal{T}$, which is typically over more than a year, but in this study is the extent of the measurement period, $\mathcal{T} \approx 7$ months. Note that both u' and $\tilde{u}$ have zero mean.

2.5 Forecast error decomposition

We will denote the root mean square difference between two wind speeds (observed and predicted, or observed at two different locations) ϵ.

For the forecasting problem in focus of this study, ultimately what matters is the velocity difference between the observed and predicted wind at the wind turbine location, $u_o(\mathbf{x}_T, t_T)$ and $u_p(\mathbf{x}_T, t_T)$ respectively. However, since the predicted wind is normally a function of both NWP forecast and previous observations, relevant to the problem is also the modelled wind (by NWP), $u_m(\mathbf{x}_T, t_T)$, and the observed wind at a different location at location on r distance and at $t - \delta t$, $u_o(\mathbf{x}_T + r, t_T - \delta t)$. When using an onsite observation in combination with NWP to predict the wind, the observation will contain unpredictable variance that will act to increase the prediction error. The magnitude of this effect depends on the scale of τ in relation to the integral time scale of the wind. To alleviate this, a series of previous observations can be utilized in the prediction to smoothen the observed signal. Thus, the squared difference between the observed wind at different times becomes relevant

$$\langle [\overline{u}(\mathbf{x}, t) - \overline{u}(\mathbf{x}, t - n\delta t)]^2 \rangle = 2\sigma_{\tilde{u}}^2 (1 - \rho(t, n\delta t)) \tag{3}$$

where n is the number of previous observation blocks considered, $\sigma_{\tilde{u}}^2 = \langle \tilde{u}^2 \rangle$ is the variance of $\tilde{u}$ and ρ is the autocorrelation function.

Since the type of onsite wind observation considered for this study is inevitably located at some distance from the target turbine(s), the RMSE between two locations will also be relevant. It can be estimated through the structure function

$$S_{\overline{u}} = \langle [\overline{u}(\mathbf{x}, t) - \overline{u}(\mathbf{x} + \mathbf{r}, t)]^2 \rangle = 2\sigma_{\tilde{u}}^2 (1 - R(\mathbf{x}, \mathbf{x} + r)), \tag{4}$$

where R is the cross correlation function. Using Taylor's frozen turbulence assumption, a temporal difference can also be expressed in terms of distance, $r \approx \overline{u}\delta t$.

For the final target prediction it is useful to expand the squared difference:

$$\langle [\overline{u}_o - \overline{u}_m]^2 \rangle = 2\sigma_{\tilde{u}_o}\sigma_{\tilde{u}_m} \left(\frac{1}{2}\frac{\sigma_{\tilde{u}_o}}{\sigma_{\tilde{u}_m}} + \frac{1}{2}\frac{\sigma_{\tilde{u}_m}}{\sigma_{\tilde{u}_o}} - R(\tilde{u}_o, \tilde{u}_m) \right), \tag{5}$$

where the assumption has been made that the long term predicted mean is equal to the observed. This is often the case

by definition since a bias correction is normally involved in the determination of the predicted wind. A difference between equations 3 and 4 to equation 5 is the first two terms. For a very high resolution model system the modelled variance will approach that of the observed variance and the expression will take the same shape as equations 3 and 4, but normally the modelled variance is lower. This has two effects, first a reduction of the sum of the two first terms, which acts to reduce the error by smoothing, and second, a reduction of the covariance term which acts to increase the error. Seen this way, an aim with the NWP input is to generate as much correlation as possible, while minimizing variance on scales that lack correlation. This illustrates the attractiveness of using a the median of a high resolution ensemble as NWP source, since the model resolution can be kept high, which better represents the physics, while still maintaining an optimal balance between smoothing of effect and correlation. Furthermore, the spread of the ensemble members can still inform on the uncertainty relative to the median.

2.6 Simplified target prediction method

To predict the wind speed at the target location there is a multitude of of techniques available that combines NWP forecast with observations using statistical methods of various complexity [10]. In line with the aim of the present study to illustrate aspects of this hybrid prediction process, as opposed to make as good predictions as possible, a very simple statistical method is adopted. First, each ensemble member is bias corrected using the reduced major axis method (RMA) [17]. RMA was chosen since both observed and simulated wind speed have variance that is physical, yet not expected to be correlated between the two, because of different resolution and non-existent predictability of small scales. RMA was chosen precisely because it allows nondeterministic variation both for dependent and independent variable. The correction was calculated as

$$\overline{u}_o = k\overline{u}_m + c_1, \tag{6}$$

where k and m are given by $k = \sigma_{\overline{u}_o}/\sigma_{\overline{u}_m}$ and $c_1 = \langle \overline{u}_0 \rangle - k \langle \overline{u}_m \rangle$. The adjustment constants k and c_1 was fitted to the SODAR S5. In the next step, the final prediction was calculated as a linear combination of the RMA corrected simulated wind speed, $\overline{u}_{m^*}$ and observed wind speed at previous N time segments:

$$\overline{u}_p(\mathbf{x}, t) = a_0 \overline{u}_{m^*}(\mathbf{x}, t) + \sum_{n=n_1}^{N} a_i \overline{u}_o(\mathbf{x} + r, t - n\delta t). \tag{7}$$

The importance of the time lag between the last accessible observation and the target time was assessed by varying n_1 from 1 to 12, giving a range between 15 minutes to 2 hours.

3 Results

In order to investigate whether or not the high resolution ensemble generated sufficiently high variance the power spectra is shown in Figure 2 both as the average of the members and for the ensemble median. It can be noted that the mean of the members has slightly higher variance at higher frequencies, as expected.

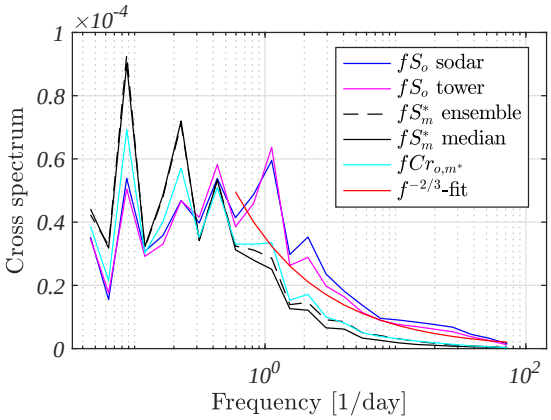

Fig. 2 Power spectra for simulated (black) and observed (blue, SODAR and magenta, tower) wind as well as cross-spectrum of the modelled and SODAR-observed wind (light blue). A -2/3 frequency dependence is shown in red for reference.

Although the difference between the observed and simulated power spectrum appears striking in Figure 2, the logarithmic axes somewhat distorts the picture and in fact the variance in the ensemble median was only 3 % lower than the observed and the average of the ratio of simulated to measured variance was 0.999 for the ensemble. Still, it is clearly visible that variance is missing at temporal scales shorter than the diurnal cycle and that the diurnal cycle itself is clearly underestimated compared to the observations. Figure 2 also displays the cross spectral density of the ensemble mean and the observations which lies close to the power spectrum of the simulations. The covariation between the observation and simulation was also assessed the trough coherence, which is presented in Figure 3, both the absolute and the its decomposition into real (simultaneous covariation, Co-coherence), and imaginary (phase lagged covariation, Quadrature-coherence) parts. As noticeable, there is little to no systematic phase lag between simulation and observation, but the scatter of the quadrature-coherence indicate that it has a strong variability and that at any scale both positive and negative phase lags exists in different times. Figure 3 also shows that on timescales shorter than 6 hours there is virtually no covariation between the simulation and observations, meaning that there is a potential to improve prediction at short lead times if the NWP is combined with site observations. As was demonstrated by 4 increasing distance between the remote sensor and the target location contributes to increased prediction errors. Figure 4 indicate that the error grows as $1 - e^{r/l_x}$ with $l_x = 30$ km. The decrease in correlation over 10 km horizontally roughly equals that of 150 m separation vertically (Figure 5).

An interesting observation is that the simulation is much more spatially correlated, horizontally and particularly vertically, than the observations. This is partly expected due to the

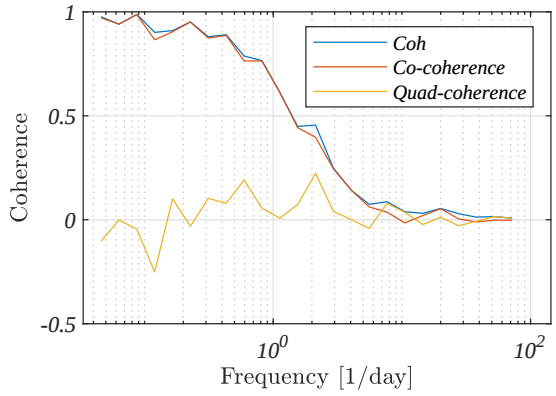

Fig. 3 Coherence of the simulated and observed wind, as well as its decomposition into Co (simultaneous) and Quadrature (phase lagged) parts.

lack of resolved turbulence, small scale terrain and surface heterogeneity.

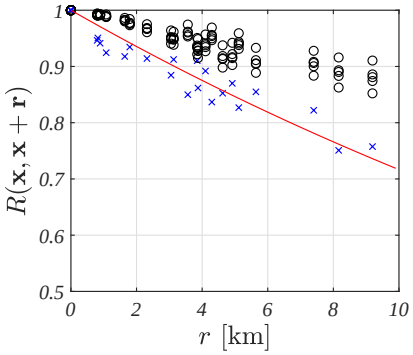

Fig. 4 Cross-correlation function of the wind at different horizontal separations, simulated, $\overline{u}_{m}*$ as black circles and observed $\overline{u}_o$. The red curve shows an exponential fit, $R = e^{-\delta x/l_x}$, with $l_x = 30$ km

A crucial aspect of using an independent wind observation to assist with the forecast is the time lag between the last observation and the forecast target time. The impact of that time lag was investigated through the value of coefficients used to determine the optimal (in a least squared sense) forecast according to equation 7. The resulting optimal linear combination of $u_{m^*}(t)$ and $u_o(t - n\delta t)$ is shown in Figure 6 together with the forecast RMSE relative to that of using only the NWP. Naturally the importance of the NWP forecast grows with increased lag time and it becomes the dominating term after the lag time grows to about an hour. The results also indicate that the tendency for the smoothing effect to reduce RMSE persist for about an hour, after which there is no added benefit of adding extra observations.

4 Discussion

Remote sensing observations typically have data gaps from challenging measurement conditions, increasingly so at higher

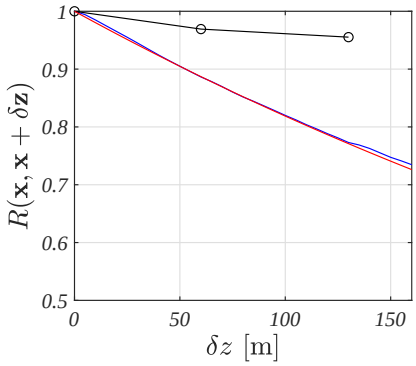

Fig. 5 Cross-correlation function of the wind at different vertical separations, simulated, $\overline{u}_{m}*$ as black circles and observed $\overline{u}_o$. The red curve shows an exponential fit, $R = e^{-\delta z/l_z}$, with $l_z = 500$ m

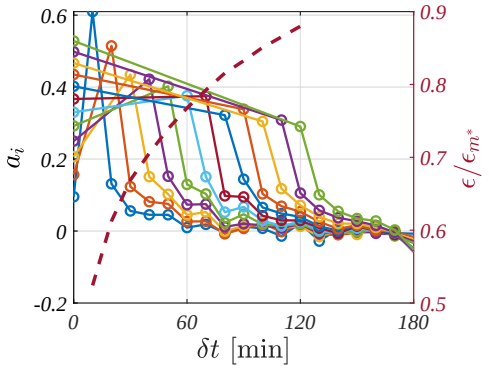

Fig. 6 Dependence of the prediction method on modelled wind $\overline{u}_{m}*$ (represented by the value at $\delta t = 0$) and previously observed wind at sets starting at different lag times. The right y-axis shows the relative reduction in prediction error by including the observations.

heights. Figures 4 and 5 can help inform whether or not it is better to turn to a previous observation or to extrapolate the wind with the most recent observation from lower height (provided measurements at lower height is available). The results indicate that a vertical extrapolation of 100 m results in roughly equal uncertainty as using a previous time step, provided the time step is 10 minutes, the wind speed is around 10 m/s and Taylor's hypothesis hold. An important observation is that the horizontal correlation length is considerable shorter than most of the reports from the literature [18], which calls for further research.

The results from the time lag analysis clearly points to that if an observational point is missing and a longer time lag temporally has to be used, the statistical model should be adjusted, putting more weight on the forecast and less on the observations. This points to the advantage of gap-filling missing data from lower heights as long as that is possible.

4.1 Limitations of the study and directions for further resarch

A limitation of the current study is the omission of the impact of wind direction relative to the separation vector. The power spectra of the observation showed clear diurnal cycles and further research that clarifies how the behaviour of correlation statistics differ between day and night would be helpful when constructing statistical prediction methods that combine onsite observations and NWP forecasts.
In this study, only a single averaging time of 10 minutes was applied, research that quantifies how the averaging time impacts correlation statistics would be useful.
A clear direction for further research is adding observed wind power data and nacelle anemometers to the prediction method. Comparing the improvement in prediction skill with and without an independent remote sensor would facilitate a true quantification of the added value of independent wind measurements. This study instead contributes to the understanding of how the placement and availability of such a remote sensor impacts its usefulness.

5 Conclusion

High-resolution systems are costly, and traditional metrics (MAE, RMSE, etc.) often fail to show clear benefits. This study have shown that as the resolution increase in the NWP model it becomes more important to provide smoothing of non-predictive variance in order minimize the prediction error. The smoothing is ideally applied using statistical measures of an ensemble, such as the mean or median, but a linear combination of previous time stamps and/or a spatial average is also beneficial and could be a particularly good option if the NWP is deterministic. The study has presented data that contributes to the understanding of which aspects of the remote sensor, such as real time availability and distance to the target location impacts the expected forecast uncertainty.

6 Acknowledgements

This work is part of the project EARS4WindEnergy - Ensemble-based approach utilizing a refinded SODAR for Wind Energy applications - funded by the European Commission's EUREKA Eurostar III - Call 3 program under the contract no. E2442, 2023-2026. All authors want to acknowledge the funding in full or in parts by the EARS4WindEnergy project.

7 References

[1] I. E. A. (IEA), Integrating solar and wind, online; accessed July 24, 2025. (September 2024).
URL https://www.iea.org/reports/integrating-solar-and-wind

[2] R. Tawn, J. Browell, A review of very short-term wind and solar power forecasting, Renewable and Sustainable Energy Reviews 153 (2022) 111758. doi:https://doi.org/10.1016/j.rser.2021.111758.
URL https://www.sciencedirect.com/science/article/pii/S1364032121010285

[3] A. Carpentieri, D. Folini, J. Leinonen, A. Meyer, Extending intraday solar forecast horizons with deep generative models, Applied Energy 377 (2025) 124186. doi:https://doi.org/10.1016/j.apenergy.2024.124186.
URL https://www.sciencedirect.com/science/article/pii/S0306261924015691

[4] E. C. J. R. Centre., Clean Energy Technology Observatory, Wind energy in the European Union: status report on technology development, trends, value chains and markets: 2024., Publications Office, LU, 2024. doi:10.2760/0882709.
URL https://data.europa.eu/doi/10.2760/0882709

[5] B. Hoen, R. Darlow, R. Haac, J. Rand, K. Kaliski, Effects of land-based wind turbine upsizing on community sound levels and power and energy density, Applied Energy 338 (2023) 120856. doi:https://doi.org/10.1016/j.apenergy.2023.120856.
URL https://www.sciencedirect.com/science/article/pii/S0306261923002209

[6] F. Theuer, M. F. van Dooren, L. von Bremen, M. Kühn, Minute-scale power forecast of offshore wind turbines using long-range single-doppler lidar measurements, Wind Energy Science 5 (4) (2020) 1449–1468. doi:10.5194/wes-5-1449-2020.
URL https://wes.copernicus.org/articles/5/1449/2020/

[7] I. Würth, L. Valldecabres, E. Simon, C. Möhrlen, B. Uzunoglu, C. Gilbert, G. Giebel, D. Schlipf, A. Kaifel, Minute-scale forecasting of wind power - results from the collaborative workshop of iea wind task 32 and 36, Energies 12 (4) (2019) 712. doi:10.3390/en12040712.
URL http://dx.doi.org/10.3390/en12040712

[8] F. Theuer, M. F. van Dooren, L. von Bremen, M. Kühn, Minute-scale power forecast of offshore wind turbines using long-range single-doppler lidar measurements, Wind Energy Science 5 (4) (2020) 1449–1468. doi:10.5194/wes-5-1449-2020.
URL https://wes.copernicus.org/articles/5/1449/2020/

[9] L. Valldecabres, N. G. Nygaard, L. Vera-Tudela, L. Von Bremen, M. Kühn, On the use of dual-doppler radar measurements for very short-term wind power forecasts, Remote Sensing 10 (11) (2018) 1701. doi:10.3390/rs10111701.
URL http://dx.doi.org/10.3390/rs10111701

[10] F. Li, H. Wang, D. Wang, D. Liu, K. Sun, A review of wind power prediction methods based on multi-time scales., Energies (19961073) 18 (7) (2025).

[11] M. Mohr, J. Arnqvist, H. Abedi, H. Alfredsson, M. Baltscheffsky, H. Bergström, I. Carlen, L. Davidson, A. Segalini, S. Söderberg, Wind power in forests ii: Forest

wind, Tech. Rep. 2018:499, Energiforsk, energiforskrapport (2018).

[12] J. Mann, N. Angelou, J. Arnqvist, D. Callies, E. Cantero, R. C. Arroyo, M. Courtney, J. Cuxart, E. Dellwik, J. Gottschall, et al., Complex terrain experiments in the new european wind atlas, Philosophical Transactions of the Royal Society A: Mathematical, Physical and Engineering Sciences 375 (2091) (2017) 20160101.

[13] C. Torrence, G. P. Compo, A practical guide to wavelet analysis, Bulletin of the American Meteorological society 79 (1) (1998) 61–78.

[14] C. Möhrlen, A. J. Jørgensen, J.U., Quality-assessment of high-resolution weather forecasts and gap-filling of real-time measurements for improved predictability in extreme events, in: Proceedings of the 23th International Wind and Solar Integration Workshop, 2024.
URL https://usercontent.one/wp/iea-wind.org/wp-content/uploads/2024/10/5D_1_WISO24_208_presentation_Moehrlen_Corinna_Online.pdf

[15] N. C. for Environmental Prediction (NCEP), The global forecast system (gfs), online; accessed Sept. 15, 2025.
URL https://www.emc.ncep.noaa.gov/emc/pages/numerical_forecast_systems/gfs.php

[16] C. Möhrlen, J. Jørgensen, The Role of Ensemble Forecasting in Integrating Renewables into Power Systems: From Theory to Real-Time Applications, no. 1 in Power Electronics and Power Systems, Springer International Publishing, 2017, Ch. 3, pp. 79–134. doi:10.1007/978-3-319-55581-2.

[17] E. B. Woolley, The method of minimized areas as a basis for correlation analysis, Econometrica: Journal of the Econometric Society (1941) 38–62.

[18] C. M. S. Martin, J. K. Lundquist, M. A. Handschy, Variability of interconnected wind plants: correlation length and its dependence on variability time scale, Environmental Research Letters 10 (4) (2015) 044004.